In mice, which do not have a fetal stage of erythropoiesis, the KLF1/BCL11A circuit affects embryonic rather than fetal gene expression.[40] This pathway normally suppresses embryonic globin synthesis in definitive erythroid cells, but a knockout of *Klf1* appears to have no effect on embryonic globins in primitive erythropoiesis, when they are normally expressed. In this model, definitive cells are not produced to determine whether or not the embryonic genes are correctly suppressed later in development.[5] It was reported anecdotally that a patient with congenital dyserythropoietic anemia type 4 and the E325K mutation had raised levels of embryonic globins. Here we show that in compound *KLF1* heterozygotes, human embryonic (ζ and ε) globin expression persists in adults. This indicates that KLF1 also plays a role in repressing embryonic globin expression in humans. This finding is striking because reactivation of embryonic globin is virtually never seen in other erythroid disorders. At present, the pathway underlying embryonic globin repression is poorly understood. However, it has recently been shown that 2 members of the KLF family (KLF3 and KLF8) may be involved in regulating embryonic globin expression, and a knockout of these 2 transcription factors in erythroid cells de-represses embryonic globin synthesis.[41] Because expression of these 2 factors is driven by KLF1, it is possible that mutations in this protein might reduce KLF3 and KLF8, leading to derepression of embryonic globins. Further analysis of this pathway is warranted because preliminary studies in mice suggest that persistence of embryonic globin expression could ameliorate severe hemoglobinothathies.[42]

In conclusion, we have shown that a wide spectrum of unexplained forms of severe inherited anemia may be caused by *trans*-acting mutations in the key erythroid transcription factor KLF1. Most remarkably, in every case where the downregulation is sufficiently severe to cause anemia, there is an associated persistence of embryonic globin expression revealing a new pathway by which globin gene expression might be manipulated to ameliorate other inherited hemoglobinopathies.

Acknowledgments

We thank all patients and parents for their participation in this study and their permission to report our findings. We also thank Helena Ayyub, Douglas Vernimmen, Ram Malladi, Katalin di Gleria, Jennifer Eglinton, and Portep Tanyut for technical support and Professor Wachara Kasinlerk of Chiang Mai University, Thailand, for the anti-ζ antibody used in this study. This work was supported by a research and development grant to V.V. by the Faculty of Medicine Siriraj Hospital and MRC Molecular Haematology Unit, Oxford, United Kingdom (to D.R.H.). S.E. and V.V. were supported by the Royal Golden Jubilee PhD program (Grant PHD/0089/2548). S.R. and N.C. received their Masters' thesis funding from tbe Department of Immunology, Siriraj Hospital. V.V. is also supported by a grant from the National Research University, Thailand, through Mahidol University and BIOTEC, Thailand. S.P. received funding from the Landsteiner Foundation for Blood Transfusion Research (LSBR 1040), the Netherlands Scientific Organization (NWO DN 82-301 and ZonMw 912-07-019 and 912-12-128) and the European Union fp7-health-2012 collaborative project THALAMOSS (306201).

Authorship

Contribution: V.V. served as the principle investigator of this study and contributed to case identification, patient care, study design, conducting the study, analysis of the data, and drafting the manuscript; S.E., S.R., N.C., C.F., K.L., H.K., S.B., and J.S. performed laboratory and DNA analysis; M.J., K.S., and V.S.T. took care of patients and collected samples; C.B. and D.S. prepared the manuscript; R.J.G., S.P., and D.R.H. provided support, research direction, and study plan and prepared the manuscript and provided mentorship; and all authors contributed to the data review and provided their comments on the manuscript.

Conflict-of-interest disclosure: The authors declare no competing financial interests.

Correspondence: Vip Viprakasit, Division of Hematology/Oncology, Department of Pediatrics and Thalassemia Center, Faculty of Medicine Siriraj Hospital, Mahidol University, 2 Prannok Road, Bangkoknoi, Bangkok 10700, Thailand; email: vip.vip@mahidol.ac.th.

References

1. McLean E, Cogswell M, Egli I, Wojdyla D, de Benoist B. Worldwide prevalence of anaemia, WHO Vitamin and Mineral Nutrition Information System, 1993-2005. *Public Health Nutr.* 2009; 12(4):444-454.
2. Modell B, Darlison M. Global epidemiology of haemoglobin disorders and derived service indicators. *Bull World Health Organ.* 2008;86(6): 480-487.
3. Borg J, Papadopoulos P, Georgitsi M, et al. Haploinsufficiency for the erythroid transcription factor KLF1 causes hereditary persistence of fetal hemoglobin. *Nat Genet.* 2010;42(9):801-805.
4. Zhou D, Liu K, Sun CW, Pawlik KM, Townes TM. KLF1 regulates BCL11A expression and gamma- to beta-globin gene switching. *Nat Genet.* 2010; 42(9):742-744.
5. Siatecka M, Bieker JJ. The multifunctional role of EKLF/KLF1 during erythropoiesis. *Blood.* 2011; 118(8):2044-2054.
6. Gallienne AE, Dréau HM, Schuh A, Old JM, Henderson S. Ten novel mutations in the erythroid transcription factor KLF1 gene associated with increased fetal hemoglobin levels in adults. *Haematologica.* 2012;97(3):340-343.
7. Satta S, Perseu L, Moi P, et al. Compound heterozygosity for KLF1 mutations associated with remarkable increase of fetal hemoglobin and red cell protoporphyrin. *Haematologica.* 2011; 96(5):767-770.
8. Pilon AM, Arcasoy MO, Dressman HK, et al. Failure of terminal erythroid differentiation in EKLF-deficient mice is associated with cell cycle perturbation and reduced expression of E2F2. *Mol Cell Biol.* 2008;28(24):7394-7401.
9. Siatecka M, Sahr KE, Andersen SG, Mezei M, Bieker JJ, Peters LL. Severe anemia in the Nan mutant mouse caused by sequence-selective disruption of erythroid Kruppel-like factor. *Proc Natl Acad Sci USA.* 2010;107(34):15151-15156.
10. Babbs C, Roberts NA, Sanchez-Pulido L, et al; WGS500 Consortium. Homozygous mutations in a predicted endonuclease are a novel cause of congenital dyserythropoietic anemia type I. *Haematologica.* 2013;98(9):1383-1387.
11. Dgany O, Avidan N, Delaunay J, et al. Congenital dyserythropoietic anemia type I is caused by mutations in codanin-1. *Am J Hum Genet.* 2002; 71(6):1467-1474.
12. Nichols KE, Crispino JD, Poncz M, et al. Familial dyserythropoietic anaemia and thrombocytopenia due to an inherited mutation in GATA1. *Nat Genet.* 2000;24(3):266-270.
13. Sankaran VG, Ghazvinian R, Do R, et al. Exome sequencing identifies GATA1 mutations resulting in Diamond-Blackfan anemia. *J Clin Invest.* 2012; 122(7):2439-2443.
14. Tachavanich K, Tanphaichitr VS, Utto W, Viprakasit V. Rapid flow cytometric test using eosin-5-maleimide for diagnosis of red blood cell membrane disorders. *Southeast Asian J Trop Med Public Health.* 2009;40(3):570-575.
15. Tachavanich K, Viprakasit V, Pung-Amritt P, Veerakul G, Chansing K, Tanphaichitr VS. Development of a comprehensive red blood cell enzymopathy laboratory in Thailand: the study of normal activity in eight erythroenzymes in Thais. *Southeast Asian J Trop Med Public Health.* 2009; 40(2):317-326.
16. Mundee Y, Bigelow NC, Davis BH, Porter JB. Simplified flow cytometric method for fetal hemoglobin containing red blood cells. *Cytometry.* 2000;42(6):389-393.

17. Chong SS, Boehm CD, Higgs DR, Cutting GR. Single-tube multiplex-PCR screen for common deletional determinants of alpha-thalassemia. *Blood.* 2000;95(1):360-362.
18. Chan AY, So CC, Ma ES, Chan LC. A laboratory strategy for genotyping haemoglobin H disease in the Chinese. *J Clin Pathol.* 2007;60(8):931-934.
19. Harteveld CL, Voskamp A, Phylipsen M, et al. Nine unknown rearrangements in 16p13.3 and 11p15.4 causing alpha- and beta-thalassaemia characterised by high resolution multiplex ligation-dependent probe amplification. *J Med Genet.* 2005;42(12):922-931.
20. Kanno H, Fujii H, Hirono A, Miwa S. cDNA cloning of human R-type pyruvate kinase and identification of a single amino acid substitution (Thr384——Met) affecting enzymatic stability in a pyruvate kinase variant (PK Tokyo) associated with hereditary hemolytic anemia. *Proc Natl Acad Sci USA.* 1991;88(18):8218-8221.
21. Singleton BK, Burton NM, Green C, Brady RL, Anstee DJ. Mutations in EKLF/KLF1 form the molecular basis of the rare blood group In(Lu) phenotype. *Blood.* 2008;112(5):2081-2088.
22. Fibach E. Techniques for studying stimulation of fetal hemoglobin production in human erythroid cultures. *Hemoglobin.* 1998;22(5-6):445-458.
23. De Gobbi M, Anguita E, Hughes J, et al. Tissue-specific histone modification and transcription factor binding in α globin gene expression. *Blood.* 2007;110(13):4503-4510.
24. Pfaffl MW. The ongoing evolution of qPCR. *Methods.* 2010;50(4):215-216.
25. Thein SL, Wood WG. In: Steinberg MH, Forget BG, Higgs DR, Weatherall DJ, eds. *The molecular basis of β thalassemia, δβ thalassemia and hereditary persistence of fetal hemoglobin. Disorders of hemoglobin.* 2nd ed. Cambridge: Cambridge University Press; 2009:323-356.
26. Prchal JT, Gregg XT. Red cell enzymes. *Hematology (Am Soc Hematol Educ Program).* 2005;19-23.
27. Helias V, Saison C, Peyrard T, et al. Molecular analysis of the rare in(Lu) blood type: toward decoding the phenotypic outcome of haploinsufficiency for the transcription factor KLF1. *Hum Mutat.* 2013;34(1):221-228.
28. Tallack MR, Whitington T, Yuen WS, et al. A global role for KLF1 in erythropoiesis revealed by ChIP-seq in primary erythroid cells. *Genome Res.* 2010;20(8):1052-1063.
29. Su MY, Steiner LA, Bogardus H, et al. Identification of biologically relevant enhancers in human erythroid cells. *J Biol Chem.* 2013;288(12):8433-8444.
30. Esteghamat F, Gillemans N, Bilic I, et al. Erythropoiesis and globin switching in compound Klf1:Bcl11a mutant mice. *Blood.* 2013;121(13):2553-2562.
31. Arnaud L, Saison C, Helias V, et al. A dominant mutation in the gene encoding the erythroid transcription factor KLF1 causes a congenital dyserythropoietic anemia. *Am J Hum Genet.* 2010;87(5):721-727.
32. Perkins AC, Sharpe AH, Orkin SH. Lethal beta-thalassaemia in mice lacking the erythroid CACCC-transcription factor EKLF. *Nature.* 1995;375(6529):318-322.
33. Turner J, Crossley M. Mammalian Krüppel-like transcription factors: more than just a pretty finger. *Trends Biochem Sci.* 1999;24(6):236-240.
34. Singleton BK, Lau W, Fairweather VS, et al. Mutations in the second zinc finger of human EKLF reduce promoter affinity but give rise to benign and disease phenotypes. *Blood.* 2011;118(11):3137-3145.
35. Borg J, Patrinos GP, Felice AE, Philipsen S. Erythroid phenotypes associated with KLF1 mutations. *Haematologica.* 2011;96(5):635-638.
36. Sankaran VG. Targeted therapeutic strategies for fetal hemoglobin induction. *Hematology (Am Soc Hematol Educ Program).* 2011;2011:459-465.
37. Satta S, Perseu L, Maccioni L, Giagu N, Galanello R. Delayed fetal hemoglobin switching in subjects with KLF1 gene mutation. *Blood Cells Mol Dis.* 2012;48(1):22-24.
38. Perseu L, Satta S, Moi P, et al. KLF1 gene mutations cause borderline HbA(2). *Blood.* 2011;118(16):4454-4458.
39. Sankaran VG, Nathan DG. Reversing the hemoglobin switch. *N Engl J Med.* 2010;363(23):2258-2260.
40. Sankaran VG, Xu J, Ragoczy T, et al. Developmental and species-divergent globin switching are driven by BCL11A. *Nature.* 2009;460(7259):1093-1097.
41. Funnell AP, Mak KS, Twine NA, et al. Generation of mice deficient in both KLF3/BKLF and KLF8 reveals a genetic interaction and a role for these factors in embryonic globin gene silencing. *Mol Cell Biol.* 2013;33(15):2976-2987.
42. Russell JE, Liebhaber SA. Reversal of lethal alpha- and beta-thalassemias in mice by expression of human embryonic globins. *Blood.* 1998;92(9):3057-3063.

Metabolism:

Deficiency of Nicotinamide Mononucleotide Adenylyltransferase 3 (Nmnat3) Causes Hemolytic Anemia by Altering the Glycolytic Flow in Mature Erythrocytes

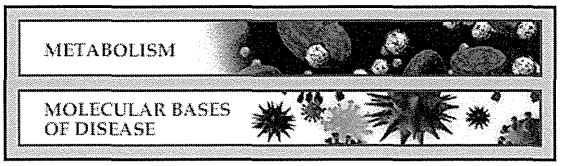

Keisuke Hikosaka, Masashi Ikutani, Masayuki Shito, Kohei Kazuma, Maryam Gulshan, Yoshinori Nagai, Kiyoshi Takatsu, Katsuhiro Konno, Kazuyuki Tobe, Hitoshi Kanno and Takashi Nakagawa

J. Biol. Chem. published online April 16, 2014

JBC Papers in Press. Published on April 16, 2014 as Manuscript M114.554378
The latest version is at http://www.jbc.org/cgi/doi/10.1074/jbc.M114.554378

Deficiency of Nicotinamide Mononucleotide Adenylyltransferase 3 (Nmnat3) Causes Hemolytic Anemia by Altering the Glycolytic Flow in Mature Erythrocytes

Keisuke Hikosaka[1], Masashi Ikutani[2], Masayuki Shito[5], Kohei Kazuma[4], Maryam Gulshan[1,3], Yoshinori Nagai[2,8], Kiyoshi Takatsu[2,7], Katsuhiro Konno[4], Kazuyuki Tobe[3], Hitoshi Kanno[5,6] and Takashi Nakagawa[1*]

[1]Frontier Research Core for Life Sciences; [2]Department of Immunobiology and Pharmacological Genetics, Graduate School of Medicine and Pharmaceutical Science for Research; [3]The First Department of Internal Medicine, Graduate School of Medicine and Pharmaceutical Science for Research; [4]Institute of Natural Medicine, University of Toyama, Toyama 930-0194, Japan; [5]Department of Transfusion Medicine and Cell Processing; [6]Department of Advanced Biomedical Engineering and Science, Graduate School of Medicine, Tokyo Women's Medical University, Tokyo 162-8666, Japan; [7]Toyama Prefectural Institute for Pharmaceutical Research, Toyama 939-0363, Japan; [8]JST, PRESTO, Saitama 332-0012, Japan

Running Title: Nmnat3 deficiency causes hemolytic anemia

Address Correspondence to: Takashi Nakagawa; Frontier Research Core for Life Sciences, University of Toyama; 2630 Sugitani, Toyama, Toyama 930-0194, Japan; Phone: +81-76-415-8849; FAX: +81-76-415-8849; E-mail: nakagawa@med.u-toyama.ac.jp

Keywords: Nicotinamide adenine dinucleotide, Nicotinamide mononucleotide adenylyltransferase 3, hemolytic anemia, glycolysis, metabolomics

---

Background: Nmnat3 is considered a mitochondria-localized NAD synthesis enzyme. However, its physiological function *in vivo* remains unclear.
Results: Loss of Nmnat3 results in drastic depletion of the NAD pool and stalls the glycolytic flow in mature erythrocytes.
Conclusion: Nmnat3 deficiency causes splenomegaly and hemolytic anemia in mice.
Significance: This report reveals the essential role of Nmnat3 in mature erythrocytes.

ABSTRACT

NAD biosynthesis is of substantial interest owing to its important roles in regulating various biological processes. Nicotinamide mononucleotide adenylyltransferase 3 (Nmnat3) is considered a mitochondria-localized NAD synthesis enzyme involved in *de novo* and salvage pathways. Although the biochemical properties of Nmnat3 are well documented, its physiological function *in vivo* remains unclear. In this study, we demonstrated that Nmnat3 was localized in the cytoplasm of mature erythrocytes and critically regulated their NAD pool. Deficiency of Nmnat3 in mice caused splenomegaly and hemolytic anemia, which was associated with the findings that Nmnat3-deficient erythrocytes had markedly lower ATP levels and shortened lifespans. However, NAD level in other tissues were not apparently affected by the deficiency of Nmnat3. LC-MS/MS based metabolomics revealed that the glycolysis pathway in Nmnat3-deficient erythrocytes was blocked at glyceraldehyde 3-phosphate dehydrogenase (GAPDH) step because of the shortage of co-enzyme NAD. Stable isotope tracer analysis further demonstrated that deficiency of Nmnat3 resulted in glycolysis stall and a shift to pentose phosphate pathway. Our

findings indicate the critical roles of Nmnat3 in maintenance of the NAD pool in mature erythrocytes and the physiological impacts at its absence in mice.

Nicotinamide adenine dinucleotide (NAD) is an important coenzyme involved in numerous metabolic enzymatic reactions including glycolysis, β-oxidation, and the tricarboxylic acid (TCA) cycle (1). NAD also serves as a substrate for poly (ADP-ribose) polymerases (PARPs) and the class III NAD-dependent deacetylases (sirtuins), and plays key roles in diverse biological processes in response to cellular stresses, including genotoxic and nutrient stress (2). The NAD level in the cell is vital for facilitating sirtuin functions as energy sensors: upon fasting or calorie restriction (3). In particular, sirtuins deacetylate central metabolic enzymes and directly control their enzymatic activities (4,5). In addition, nuclear sirtuins can indirectly regulate central metabolic pathways by deacetylating diverse transcriptional factors and cofactors including FOXO, PPAR, and PGC1α (6-8). Recent studies indicate that NAD metabolism also regulates various biological processes via NAD-dependent deacetylase SIRT1 (9-11). However, there is no direct evidence that NAD metabolism can regulate metabolic enzymes that requires NAD as a coenzyme.

In organisms, NAD can be synthesized via a *de novo* synthesis pathway or a salvage pathway (12). In the salvage pathway, Nicotinamide phosphoribosyltransferase (Nampt) converts nicotinamide (NAM) and phosphoribosyl pyrophosphate (PRPP) to nicotinamide mononucleotide (NMN). Then, nicotinamide mononucleotide adenylyltransferase (Nmnat) transfers the adenylyl moiety from ATP to NMN for generating NAD (12). In mammals, there are three Nmnat isoforms (Nmnat1–3) with different subcellular localizations and tissue distributions (13,14). Nmnat1, Nmnat2, and Nmnat3 are considered to be localized in the nucleus, Golgi apparatus, and mitochondria, respectively. Nmnat1 has the most robust enzymatic activity of the three isoforms (13). A recent genetic study revealed that *Nmnat1* gene mutations cause Leber congenital amaurosis, a rare hereditary blindness (15-18). *Nmnat1* is also identified as a fusion gene with *Ube4b* in Wallerian degeneration slow (WldS) mice, which exhibit drastic delays in injured axonal clearance (19). Indeed, Nmnat1 overexpression in mice is protective against sciatic nerve injury (20). Although Nmnat1 has important roles in central and peripheral nervous system, its protein expression level is relatively low compared with that of Nmnat2 (21). Several papers have suggested the implication of Nmnat2 in axonal cell survival and protection (22,23). Nmnat1 and Nmnat2 also have essential roles in axonal growth and survival during embryogenesis as their deficiency in mice results in embryonic lethal. (21,24,25).

Nmnat3 has been considered to be localized in mitochondria and to have a pivotal role in regulation of mitochondrial NAD level (13,26). Despite the importance of NAD metabolism in mitochondria, the role of Nmnat3 *in vivo* is still unclear. Nmnat3 overexpression confers robust protection against axon injury *in vitro* and *in vivo* as well as WldS chimeric protein (27,28). Although the significance of Nmnat3 in axonal protection is evident, the molecular mechanism is still unknown, as for the case of Nmnat1.

It has long been suspected if red blood cells (RBCs) possess NAD synthesis activity (29,30). Several reports have indicated that RBCs show Nmnat-like activity (31-34), but the actual identity of responsible enzymes has been uncertain. Magni's group, employing a Nmnat discrimination assay, found Nmnat3-specific activity in human RBCs (35). However, given that RBCs have no mitochondria in cells, it has not been clarified whether Nmnat3 has a physiological function in RBCs. In this study, we found that Nmnat3-deficient mice exhibited splenomegaly and hemolytic anemia resulting from a glycolysis pathway blockade at glyceraldehyde 3-phosphate dehydrogenase (GAPDH). Our findings revealed unexpected roles of Nmnat3 in the maintenance of the NAD pool in mature erythrocytes and their lifespan regulation.

EXPERIMENTAL PROCEDURES

Generation of Nmnat3 gene trap mice - Nmnat3 gene-trap heterozygous frozen embryo was

obtained from TG Resource Bank (Transgenic Inc. Japan) and embryonic transfer was performed to get gene-trap heterozygous mice. To determine the precise inserted location of gene-trap cassette in the *Nmnat3* gene, the genomic walking was carried out using GenomeWalker Universal Kit (Takara, Japan). After confirming the accurate insertion point of gene-trap cassette, we designed primer sets for genotyping as shown in Table 1. Nmnat3 gene-trap homozygous ($Nmnat3^{gt/gt}$) mice were obtained by crossing heterozygous mice. Mice were maintained under controlled temperature and standard light conditions (12h:12h light-dark cycle) and were allowed free access to water and food. All animal experiments were approved by the Animal Experiment Committee at University of Toyama and were carried out in accordance with the Guidelines for the Care and Use of Laboratory Animals at University of Toyama, which were based on international policies.

Real-time quantitative PCR (qPCR) - Total RNAs were extracted from mice tissues using TRI Reagent (Molecular Research Center, Inc.). cDNA was prepared using ReverTra Ace qPCR RT Master Mix with gDNA Remover (Toyobo, Japan) according to the supplier's protocol. Real-time PCR was carried out using THUNDERBIRD SYBR qPCR Mix (Toyobo) on Thermal Cycler Dice Real Time System II (Takara). Quantification was done by Delta Delta Ct method, and *Rpl13a* or *B2m* gene was used as a reference gene. Primers used in qPCR are listed in Table 1.

Preparation of mature erythrocytes - Mature erythrocytes were separated by a Percoll gradient method according to a standard protocol (36). Briefly, Percoll solution of densities at 1.096 and 1.058 g/ml were prepared. 2 ml of Percoll solution (density, 1.096 g/ml) was added at the bottom, followed by 1 ml of Percoll (density, 1.058 g/ml) layered on top. Finally, 1 ml of whole blood was applied onto the gradient, followed by centrifuge at 250 x *g* for 30 min. Mature erythrocytes packed in the bottom of layer were collected carefully and washed with ice-cold saline.

Western blotting experiments - Mature erythrocytes isolated by a Percoll gradient were lysed with NP-40 lysis buffer (150 mM NaCl, 1.0% NP-40, and 50 mM Tris-HCl, pH 7.4), and were subjected to Western blotting. For fractionation experiments, hemolysed samples were used as cytoplasm fraction and ghost was used as membrane fraction. Whole blood was centrifuged at 1,000 x *g* for 5 min at room temperature, and then plasma and buffy coat were discarded. Erythrocytes were lysed with 5 mM sodium phosphate buffer (pH 8.0) on ice for 30 min and centrifuged at 20,000 x *g* for 20 min at 4 °C. The supernatant was used as hemolysed sample. The pellet was washed with 5 mM sodium phosphate buffer (pH 8.0) twice and used as ghost fraction. Antibodies used for Western blotting experiments included Nmnat1 (Novus), Nmnat2 (Sigma), GAPDH (Sigma), PFK (Abcam), β-actin (Cell Signaling), Nampt (Bethyl), NADK (Santa Cruz), β-tubulin (Cell Signaling), Tom20 (Santa Cruz) and acetyl-lysine (Abcam and Cell Signaling). Anti-mouse Nmnat3 rat monoclonal antibody (clone R88) was raised against His-tagged full-length mouse Nmnat3 recombinant protein and spleen cells were used to make hybridoma cells by polyethylene glycol method. For Western blotting, hybridoma supernatant was used at 100 times dilution. HRP-conjugated secondary antibodies were obtained from Millipore. PVDF membrane (Millipore) was used for blotting and signals were detected by LAS4000 mini digital imager (GE Health Care).

Histological and cytological staining - All staining solutions were purchased from Muto Pure Chemicals (Japan). For HE staining, spleen was embedded in OCT (Tissue-Tek) using dry ice/acetone bath. Serial sections at 10 μm thickness were made on a cryostat (Leica CM3050S) and tissue sections were placed on the MAS coated slide glass (Matsunami, Japan). After the fixation with 4% paraformaldehyde, sections were stained with hematoxylin and eosin. For May-Giemsa staining, air-dried whole blood smear was made on MAS coated slide glass. Blood smear slides were fixed and stained with May Grunwald staining solution and Giemsa solution. For New Methylene Blue staining, two volume of blood and one volume of New Methylene Blue staining solution were mixed and incubated for 15 min at room temperature. Sample slides were observed using

BX61 microscope equipped with 100× oil-immersion lens (Olympus, Japan).

Scanning electron microscope (SEM) analysis - Blood samples were fixed with 2% glutaraldehyde in 0.1 M phosphate buffer for 1 h at 4 °C. After the samples were washed with 0.1 M phosphate buffer two times, the post fixation was carried out using 1% Osmium Tetroxide in 0.1 M phosphate buffer for 1 h at 4 °C. After the wash with 0.1 M phosphate buffer, samples were gradually dehydrated using 50%, 70%, 80%, 90%, 99% (v/v ethanol/water), and 100% ethanol for 5 min in each step. Ethanol was replaced by t-butyl alcohol and the samples were frozen at 4 °C. After vacuum drying, the surface of samples was coated with platinum/palladium. Samples were observed by field emission scanning electron microscope (FE-SEM) S-4500 (Hitachi, Japan).

Flow cytometer analysis and cell sorting experiments - Bone marrow cells were harvested from femur bones. The single-cell suspension of splenocytes and bone marrow cells were prepared by passing through a 70 μm cell-strainer (BD). Peripheral blood was obtained by tail bleeding. Ter119 and CD71 expression were examined using anti-Ter119-PE and anti-CD71-FITC conjugated antibodies (BD; 1:200 dilution). Flow-activated cell sorting (FACS) analysis was performed using a FACS Canto II Flow Cytometer (BD). Each erythroblasts population was obtained from splenocytes by FACS Aria Cell Sorter (BD).

In vivo erythrocyte lifespan assay - *In vivo* erythrocyte lifespan assay was described elsewhere (37). Briefly, 12 weeks old mice were biotinylated by tail vein injection of 3 mg EZ-Link Sulfo-NHS-biotin (Thermo) dissolved in 0.2 mL phosphate-buffered saline. After 4 h circulation, blood was drawn from the tail vein and labeled with phycoerythrin (PE)-conjugated streptavidin (1:500). The biotinylated erythrocyte was measured using FACS Canto II Flow Cytometer and calculated as 100% biotinylated erythrocyte at Day 0. Subsequently, blood was drawn at Day 3, 5, 10, 15, and 20 and the percentage of biotinylated erythrocyte was determined.

Nmnat activity and discrimination Assay - Hemolysed samples were prepared as described above. Each sample was normalized by hemoglobin concentration at 20 μg/μl, and then hemoglobin was depleted using HemogloBind (Biotech Support Group LCC.). After depletion of hemoglobin, samples were dialyzed against dialysis buffer (25 mM Tris-Cl pH 7.8, 100 mM NaCl and 10% glycerol) to remove interfering endogenous metal ions and metabolites. The condition of discrimination assay was determined by previous report (38). The total 100 μl of reaction mixture contains 10 μl of dialyzed sample, 1 mM ATP and 1 mM NMN in final concentration. Metal ions were used at 0.05 mM for $MgCl_2$ or 5 mM for $CoCl_2$ in final concentration. The reaction was terminated by adding 200 μl 0.5N perchloric acid (PCA) at 0, 10, 20, and 30 min. After centrifugation, supernatant was collected and the formed NAD amount was measured by LC-MS/MS method described below.

Enzymatic activity assay of erythrocytes metabolic enzymes - Heparinized whole blood was washed three times with ice-cold saline and passed through a column of α-cellulose and microcrystalline cellulose to deplete leukocytes and platelets. Enzyme activities in RBCs were measured by the methods recommended by International Committee for Standardization in Hematology (39).

Metabolites extraction for LC-MS/MS measurement - The metabolites of erythrocytes were extracted using PCA for NAD related metabolites except for NADH (40) or methanol for glycolysis related metabolites (41). NADH was extracted with ammonium acetate/ acetonitrile (ACN)/ chloroform (42). For PCA extraction, 400 μl of whole blood was centrifuged at 1,000 x *g* for 5 min at room temperature, and then plasma and buffy coat were discarded. Packed erythrocytes were washed with ice-cold saline twice and cell numbers were counted by automated cell counter (Invitrogen). Then, 400 μl of 0.5 N PCA was added to the packed $5x10^8$ erythrocytes. After the vortex, precipitated proteins were separated by centrifugation at 15,000 x *g* for 10 min at 4 °C. Right before the measurement, supernatant was neutralized with equal volume of 1 M ammonium formate and filtered with 0.45 μm Millex filter unit (Millipore). For

methanol extraction, 400 µl of whole blood was used for preparing packed erythrocytes. After washing with ice-cold saline twice, $5x10^8$ erythrocytes were lysed with 350 µl of LC-MS grade pure water followed by addition of 150 µl of 100% methanol. Then, samples were boiled at 95 °C for 1 min and kept on ice for 10 min. After centrifugation, collected supernatants were filtered with 0.45 µm Millex filter unit. NAD related metabolites extraction from whole blood was performed by direct PCA addition followed by the same procedure as RBC samples.

Metabolites measurement by LC-MS/MS - Metabolites level was determined by Agilent 6460 Triple Quad mass spectrometer coupled to Agilent 1290 HPLC system. Chromatographic conditions are used as previously described with modifications (40,43). NAD related metabolites were separated on Waters Atlantis T3 column (2.1 x 150 mm, 3 µm) with 10 µl volume injection and at a flow rate of 150 µl/min using 5 mM ammonium formate for mobile phase A and 100% methanol for mobile phase B. The setting for gradients was as following: 0-10 min, 0-70%B; 10-15 min, 70%B; 15-20 min, 0%B. MS was operated in positive ESI MRM mode. Absolute amount of NAD was calculated from NAD standard curve by MassHunter Quantitative analysis software (Agilent). Glycolysis related metabolites were separated on Waters XBridge Amide column (2.1 x 150 mm, 3.5 µm) with 10 µl volume injection and at a flow rate of 300 µl/min using 20 mM ammonium acetate pH 9.0 (H_2O:ACN=95:5) for mobile phase A and 100% ACN for mobile phase B. The setting for gradients was as following: 0-5 min, 85-42%B; 5-16 min, 42-2%B; 16-21 min, 2%B; 21-30 min, 85%B. MS was operated in negative ESI MRM mode. All solvents used for these experiments were LC-MS grade or HPLC grade purchased from Wako pure chemicals (Osaka, Japan).

13C-Glucose labeling and tracer analysis - Whole blood was centrifuged at 1,000 x *g* for 5 min at room temperature and plasma and buffy coat were removed. Packed erythrocytes were washed with 1 ml of physiological saline once. 2.5×10^8 cells/tube were pre-incubated with normal RPMI 1640 medium (Nacalai Tesque, Japan) at 37 °C for 30 min, then medium was changed to glucose-free RPMI 1640 medium (Nacalai Tesque) supplemented with 2.0 g/l [U-13C]-glucose or [1,2-13C]-glucose (Cambridge Isotope Inc.). The samples were collected at 0, 30, 60, 90, and 120 min after medium change. Metabolites were extracted by methanol described above.

ATP measurement - Whole blood ATP level was measured using Blood ATP measuring kit (TOYO INK, Japan), which is based on a renilla luciferase-ATP-luciferin luminescent reaction. Luminescence was measured by Varioskan Flash (Thermo) after Luciferin/Luciferase solution was injected to sample according to manufacture's instruction.

Peripheral blood cell count - For peripheral blood cell count, whole blood was collected from inferior vena cave under anesthesia. Whole blood was immediately transferred to a EDTA-2K containing tube. Peripheral blood cell count was carried out at the FALCO Bio Systems veterinary medicine laboratories (Kyoto, Japan). Reticulocyte and white blood cell subpopulations were counted by flow cytometer method at the FALCO Bio Systems veterinary medicine laboratories.

Statistic Analysis - Analysis was performed using an unpaired or paired Student's t-test, and significant differences are indicated by single asterisk (*) when $p < 0.05$, double asterisk (**) when $p < 0.01$ and triple asterisk (***) when $p<0.005$.

RESULTS

Nmnat3 is localized in cytoplasm of mature erythrocytes

The Nmnat3 protein expression pattern of wild-type mice in various tissues was examined by Western blotting, using a rat monoclonal antibody raised against the mouse Nmnat3 full-length recombinant protein. Although Nmnat3 is known to be important in mitochondrial NAD metabolism, Nmnat3 protein expression showed marked variation in the tissues (Fig. 1A). RBC showed the highest expression level among the tissues examined, and heart, skeletal muscle, and liver showed relatively lower amounts of Nmnat3 (Fig. 1A). Nmnat3 was reported as a mitochondrial protein by several previous researchers (13,26,28,44).

Indeed, we were able to confirm that overexpressed Nmnat3 was localized in mitochondria in HeLa cells (Fig. 1B). However, it is also known that mature erythrocytes have no mitochondria. We accordingly investigated the subcellular localization of Nmnat3 in mature erythrocytes. We isolated mature erythrocytes from the wild-type mice by a Percoll gradient method and then successfully fractionated mature erythrocyte proteins into cytoplasmic and membrane fractions. We found Nmnat3 exclusively in the cytoplasmic fraction of mature erythrocyte (Fig. 1C). Next, we examined the subcellular localization of Nmnat3 in reticulocyte, which possess mitochondria. We found that Nmnat3 in reticulocytes also existed in cytoplasmic fraction rather than mitochondria (Fig. 1D). From these results, we concluded that Nmnat3 is a cytoplasmic protein, at least in mature erythrocytes and reticulocytes.

Nmnat3$^{gt/gt}$ mice exhibited splenomegaly and hemolytic anemia

To investigate the physiological functions of Nmnat3, we generated Nmnat3-deficient mice by the gene-trap method (Fig. 2A-C). We verified that Nmnat3 mRNA and protein were absent in Nmnat3 gene-trap homozygous (Nmnat3$^{gt/gt}$) mice (Fig. 2D-H). Thus, Nmnat3$^{gt/gt}$ mice were considered as Nmnat3-deficient mice, or at least severely Nmnat3-scarce mice.

Nmnat3$^{gt/gt}$ mice were born in a Mendelian's ratio (data not shown) and looked normal at appearance. However, Nmnat3$^{gt/gt}$ mice exhibited splenomegaly from a young age (Fig. 2I and J), and histological examination revealed that the red pulp of the spleen was enlarged (Fig. 2K). Increased iron deposits (hemosiderin) were also seen in Nmnat3$^{gt/gt}$ mice spleens (Fig. 2K). These results suggested that erythrocyte destruction was increased in Nmnat3$^{gt/gt}$ mice. As expected, hematological examination of peripheral blood in Nmnat3$^{gt/gt}$ mice revealed moderate anemia, as evidenced by decreased numbers of RBC, lower hematocrits (Ht) and lower concentrations of hemoglobin (Hb) (Table 2). However, no significant differences were found in numbers of white blood cell (WBC) and platelets (PLT) between Nmnat3$^{gt/gt}$ and control mice. Numbers of reticulocytes in Nmnat3$^{gt/gt}$ mice were markedly increased (Table 2). We confirmed reticulocytosis in Nmnat3$^{gt/gt}$ mice by May–Giemsa staining and New Methylene Blue staining (Fig. 2L). These data suggested that Nmnat3$^{gt/gt}$ mice manifested hemolytic anemia. In support of this view, scanning electron microscopy (SEM) detected a striking morphological change in Nmnat3$^{gt/gt}$ RBCs. RBCs in control mice showed the normal discocyte shape, whereas most RBCs in Nmnat3$^{gt/gt}$ mice appeared as acanthocytes or echinocytes, which show abnormal spiked membrane projections (Fig. 2M). Next, we assessed the lifespan of erythrocytes using an *in vivo* biotin-labeling method. The lifespan of mature erythrocytes in rodents has been reported as 50 to 60 days on an average (37). However, we found the lifespan of erythrocytes in Nmnat3$^{gt/gt}$ mice to be greatly reduced to approximately 10 days (Fig. 2N). We concluded from these findings that Nmnat3$^{gt/gt}$ mice exhibited splenomegaly due to hemolytic anemia.

Erythropoiesis is upregulated in Nmnat3$^{gt/gt}$ mice as a compensatory mechanism

Nmnat3$^{gt/gt}$ mice showed increased numbers of reticulocytes (Table 2 and Fig. 2L), suggesting that erythropoiesis in these mice would be normal. In anemic mice, increased erythropoiesis primarily occurs in spleen rather than in bone marrow (45). We next investigated the erythropoiesis stage using the cell surface markers CD71 (transferrin receptor) and Ter119 (glycophorin-associating protein) in splenocytes and bone marrow cells (46). Immature CD71^{high}Ter119^{high} (P4) and CD71^{middle}Ter119^{high} (P5) fractions were markedly increased in splenocytes from Nmnat3$^{gt/gt}$ mice (Fig. 3A). However, the most mature CD71^{low}Ter119^{high} (P6) fraction was decreased. The larger P4 fraction was also observed in bone marrow cells (Fig. 3B). We further checked the erythroid developmental stage of peripheral blood. Consistent with the hematological examination, mature erythrocyte fraction (P6) was decreased in Nmnat3$^{gt/gt}$ mice (Fig. 3C). In general, reticulocytes enter the peripheral blood after enucleation and retain mitochondria. We investigated whether this step occurred normally in Nmnat3$^{gt/gt}$ mice. Peripheral blood samples from Nmnat3$^{gt/gt}$ and control mice were stained

with Hoechst 33342 and MitoTracker Orange for nucleus and mitochondria, respectively. As shown in Fig. 3D, nuclei were rarely seen in either mice, but there were more mitochondria in Nmnat3$^{gt/gt}$ mice likely due to larger fraction of reticulocytes. Taking all evidence together, we concluded that erythropoiesis was markedly increased to compensate for the decrease in mature erythrocytes, but that peripheral erythroid maturation was generally normal in Nmnat3$^{gt/gt}$ mice. These results also support the proposition that the anemia in Nmnat3$^{gt/gt}$ mice was not due to the abnormality in erythropoiesis but due to the shorter lifespan of mature erythrocytes.

Nmnat3 is a dominant Nmnat isozyme in mature erythrocytes

We found that Nmnat3 was present in mature erythrocytes and had a crucial role in their lifespan regulation. However, the significance of the two other Nmnat isozymes in mature erythrocytes is not clear. To address this question, we investigated whether enzymatic activity of the other Nmnat isoforms could be detected in mature erythrocytes. To assess Nmnat enzymatic activity, we employed an Nmnat isozyme discrimination assay (38), in which $MgCl_2$ was used as a metal cofactor to measure total Nmnat activity and $CoCl_2$ for relatively Nmnat3-specific activity. We confirmed that Nmnat3-specific activity was almost absent from Nmnat3$^{gt/gt}$ erythrocytes (Fig. 4A, Left panel). Total Nmnat activity was largely compromises as well, suggesting that the other two Nmnat activities were absent or at least very minor (Fig. 4A, Right panel). Consistent with these results, neither Nmnat1 nor Nmnat2 was identified in mature erythrocytes by Western blotting with Nmnat1- and Nmnat2-specific antibodies (Fig. 4B). These results suggested that Nmnat3 is most dominant among the three Nmnat isozymes in mature erythrocytes.

NAD pool is drastically decreased in Nmnat3$^{gt/gt}$ erythrocytes

Next, we investigated the effect of Nmnat3 deficiency on NAD metabolism in erythrocytes. We measured NAD-related metabolites in RBCs using multiple reaction monitoring (MRM)-based liquid chromatography–tandem mass spectrometry (LC-MS/MS) method. The NAD level in Nmnat3$^{gt/gt}$ erythrocytes was drastically reduced compared with that in wild-type erythrocytes (Fig. 5A and B). NADH was also markedly decreased in Nmnat3$^{gt/gt}$ erythrocytes (Fig. 5C). However, NADH/NAD ratio was not much changed (WT 0.0072; Nmnat3$^{gt/gt}$ 0.0063). To avoid the potential changes during sample preparation, we also measured NAD in whole blood samples, which were immediately quenched after blood collection from anesthetized mice. NAD levels of whole blood in Nmnat3$^{gt/gt}$ mice were reduced to the same extent as in RBCs (Fig. 5D). We also measured other NAD-related metabolites in RBCs and whole blood. NMN and NAM were markedly reduced in Nmnat3$^{gt/gt}$ erythrocytes. (Fig. 5E and F). However, nicotinic acid (NA) and tryptophan (Trp) were unchanged between WT and Nmnat3$^{gt/gt}$ RBCs. We also found that nicotinic acid dinucleotide (NAAD) was significantly reduced in Nmnat3$^{gt/gt}$ RBCs (Fig. 5E). This result confirmed the involvement of Nmnat3 in the final step of the *de novo* synthesis pathway. In addition, we measured NAD level in other tissues, such as liver, heart and skeletal muscle and surprisingly found that the level of NAD in these tissues was not changed in Nmnat3$^{gt/gt}$ mice (Fig. 5G). We also determined whether the NAD level in erythroid precursor cells was affected. We isolated P4 (polychromatophilic erythroblast, orthochromatic erythroblast and reticulocyte), P5 (reticulocyte) and P6 (mature erythrocyte) subpopulation cells from total splenocytes using a cell sorter (Fig. 5H). Consistent with the result obtained from RBCs and whole blood, the mature erythrocytes fraction (P6) from Nmnat3$^{gt/gt}$ mice had a markedly reduced NAD level. In contrast, no change was observed in the P4 or P5 fractions (Fig. 5I). These results suggested that Nmnat3 is critical for maintaining NAD levels only in mature erythrocytes and not in their precursor cells or other tissues such as heart, liver and skeletal muscle.

In erythrocytes, the pentose phosphate pathway is very active in protecting against oxidative stress through the NADP–glutathione system (47). Interestingly, we observed no significant difference in NADP level between WT and Nmnat3$^{gt/gt}$ erythrocytes (Fig. 5J). To investigate

how NADP was maintained in Nmnat3$^{gt/gt}$ erythrocytes, we examined the expression level of NAD kinase (NADK), which was responsible for generating NADP from NAD. We found that NADK was significantly increased in Nmnat3$^{gt/gt}$ erythrocytes (Fig. 5K). In addition, the concentration of NADP in erythrocyte was much less than that of NAD (Fig. 5B and J). Therefore, it was speculated that NADP in Nmnat3$^{gt/gt}$ erythrocytes was more preferentially maintained than NAD. We also found that reduced glutathione (GSH) level in Nmnat3$^{gt/gt}$ erythrocytes was comparable to that in WT. However, the oxidative glutathione (GSSG) was slightly but significantly decreased (Fig. 5L). This result also supported the idea that NADP was maintained in Nmnat3$^{gt/gt}$ erythrocytes. Taken all together, we inferred that the NADP–glutathione system in Nmnat3$^{gt/gt}$ erythrocytes was not impaired.

Glycolytic pathway was blocked in Nmnat3$^{gt/gt}$ erythrocytes

Erythrocytes are known to exclude all of organelles, including nucleus and mitochondria, during maturation. Thus, energy (as ATP) production in mature erythrocytes relies primarily on the cytosolic glycolysis pathway. In particular, glyceraldehyde-3-phosphate dehydrogenase (GAPDH) and lactate dehydrogenase (LDH) use NAD and NADH for their enzymatic reactions and recycle them between these two reactions. To assess the effect of Nmnat3 deficiency on glycolysis, we quantified metabolites of the glycolysis pathway and the pentose phosphate pathway by LC-MS/MS. Among glycolysis pathway intermediate metabolites, upstream metabolites, including glucose-6-phosphate (G6P), fructose-6-phosphate (F6P), and fructose 1,6-bisphosphate (F1,6BP) were markedly increased in Nmnat3$^{gt/gt}$ erythrocytes (Fig. 6A). In contrast, downstream metabolites, including 3-phosphoglycerate (3PG), phosphoelolpyruvate (PEP), and lactate (LAC) were significantly decreased in Nmnat3$^{gt/gt}$ erythrocytes (Fig. 6A). In addition, phosphoribosyl pyrophosphate (PRPP) was markedly increased (Fig. 6A). In the pentose phosphate pathway, ribose 5-phosphate (R5P), ribulose 5-phosphate (Ru5P), and xylulose 5-phosphate (Xu5P) were increased in Nmnat3$^{gt/gt}$ erythrocytes (Fig. 6A). These data indicated that the glycolysis pathway in Nmnat3$^{gt/gt}$ erythrocytes was blocked in the middle and that the metabolic flow was shifted to the pentose phosphate pathway.

Next, we examined enzymatic activities of various glycolytic enzymes in erythrocytes to determine how the glycolysis pathway in Nmnat3$^{gt/gt}$ erythrocytes was blocked. We measured enzymatic activities of RBC lysate with excess amounts of substrates *in vitro*. The activities of most enzymes were upregulated in Nmnat3$^{gt/gt}$ erythrocytes (Fig. 6B). For instance, phosphofructokinase (PFK), a rate-limiting enzyme of glycolysis, was markedly increased in Nmnat3$^{gt/gt}$ erythrocytes (Fig. 6B). In agreement with this finding, the protein level of PFK was also increased in Nmnat3$^{gt/gt}$ erythrocytes (Fig. 6C). We also investigated other enzymes whose deficiency causes hemolytic anemia in human patients. However, they were unchanged or even increased in Nmnat3$^{gt/gt}$ erythrocytes (Fig. 6D and E). Previous study reported that acetylation increased the enzymatic activities of certain glycolytic enzymes (4,5). In Nmnat3$^{gt/gt}$ erythrocytes, NAD levels were markedly decreased, and NAD-dependent deacetylase sirtuins may have been inactivated. Additionally, levels of acetyl-CoA, which is a substrate for acetylation, were also markedly increased in Nmnat3$^{gt/gt}$ erythrocytes (Fig. 6F). We accordingly speculated that the acetylation status of Nmnat3$^{gt/gt}$ erythrocyte proteins would be increased. We examined acetylation status by Western blotting with antibodies against acetylated-lysine residues and found that acetylation levels were indeed increased in Nmnat3$^{gt/gt}$ erythrocytes compared with that in WT (Fig. 6G). We inferred that the increased activities of several glycolytic enzymes in Nmnat3$^{gt/gt}$ erythrocytes were due in part to the increased acetylation of these enzymes.

Metabolic flow in Nmnat3$^{gt/gt}$ erythrocytes was reversed to F1,6BP through the pentose phosphate pathway.

Because glycolysis enzymes in Nmnat3$^{gt/gt}$ erythrocytes showed increased activity compared with that in WT erythrocytes, we speculated that the inhibition of glycolysis pathway in Nmnat3$^{gt/gt}$ erythrocytes was due to the blockade

at GAPDH, which uses NAD as a coenzyme for the enzymatic reaction. Metabolomics data also suggested that the glycolysis pathway in Nmnat3$^{gt/gt}$ erythrocytes was stalled between F1,6BP and 3PG (Fig. 6A). However, we confirmed that the protein levels of GAPDH were unchanged in Nmnat3$^{gt/gt}$ erythrocytes (Fig. 6C). This finding also suggested that GAPDH was inhibited due to the reduced levels of NAD. To test this hypothesis, we performed *ex vivo* stable-isotope tracer analysis using 13C-labeled glucose. Erythrocytes isolated from WT and Nmnat3$^{gt/gt}$ mice were cultured in RPMI 1640 medium supplemented with 13C-labeled glucose, and samples were collected at several time points. First, [U-13C]-glucose was employed to evaluate the total flow of the glycolysis pathway. As shown in Fig. 7A, 13C-labeled F1,6BP increased much more rapidly in Nmnat3$^{gt/gt}$ erythrocytes. R5P/Ru5P and DHAP also increased more in Nmnat3$^{gt/gt}$ erythrocytes. However, the accumulation of downstream metabolites including GAP, 2,3-BPG, 3PG and PEP was clearly slower in Nmnat3$^{gt/gt}$ erythrocytes (Fig. 7A). Thus, the glycolysis pathway in Nmnat3$^{gt/gt}$ erythrocytes was markedly slowed compared with that in WT erythrocytes.

From static metabolomics data, we observed that F1,6BP, but not GAP, was increased in Nmnat3$^{gt/gt}$ erythrocytes (Fig. 6A). [U-13C]-glucose tracer analysis also indicated that the flow became slower between F1,6BP and GAP, a step catalyzed by aldolase. However, the enzymatic activity of aldolase was not reduced in Nmnat3$^{gt/gt}$ erythrocytes (Fig. 6B). We accordingly hypothesized that the glucose flows from the pentose phosphate pathway was reversed between F1,6BP and GAP. To test this hypothesis, we used [1,2-13C]-glucose for further experiments to determine whether the flux to F1,6BP was directly from glycolysis or reversed from the pentose phosphate pathway via GAP. If F1,6BP were derived straightly from glucose, the 1,2-carbon (+2) of F1,6BP would be labeled. In contrast, if it was synthesized through the pentose phosphate pathway and reversed from GAP, the 1-carbon (+1), 1,2,4-carbon (+3) or 1,2,3,4-carbon (+4) of F1,6BP would be labeled with 13C (Fig. 7B). As shown in Fig. 7C, F1,6BP (+1), (+3) and (+4) were significantly increased in Nmnat3$^{gt/gt}$ erythrocytes, whereas the level of F1,6BP (+2) was near that of WT. Additionally, R5P/Ru5P (+1) was also increased in Nmnat3$^{gt/gt}$ erythrocytes (Fig 7D). We concluded that the glycolytic flow in Nmnat3$^{gt/gt}$ erythrocytes was blocked at GAPDH owing to the shortage of NAD. Moreover, the glycolytic flow in Nmnat3$^{gt/gt}$ erythrocytes was shifted to the pentose phosphate pathway, and the blockade at GAPDH resulted in a reverse flow into F1,6BP from GAP.

Finally, we measured the ATP level of whole blood in the WT and Nmnat3$^{gt/gt}$ mice and found that the ATP level was markedly decreased in Nmnat3$^{gt/gt}$ mice (Fig. 7E). Thus, glycolysis blockade in Nmnat3$^{gt/gt}$ erythrocytes caused ATP production failure and ultimately lead to hemolytic anemia (Fig. 8).

DISCUSSION

Although the importance of NAD metabolism in various biological processes is known, the physiological function of Nmnat3 *in vivo* is not fully understood. In this study, we demonstrated that the NAD synthesis enzyme, Nmnat3, plays an essential role in the maintenance of the NAD pool in mature erythrocytes. Given that Nmnat3 is the dominant Nmnat among the three isoforms in mature erythrocytes, its deficiency leads to a drastic depletion of the NAD pool. Mature erythrocytes have no mitochondria, and their energy metabolism relies primarily on glycolysis. Thus, a lowered NAD level inhibits glycolysis at GAPDH and their ATP production is impaired in Nmnat3$^{gt/gt}$ erythrocytes. In erythrocytes, most ATP is consumed by Na^+-K^+-ATPase, a plasma membrane-embedded pump that maintains erythrocyte shape (48). An ATP shortage in Nmnat3$^{gt/gt}$ erythrocytes leads to dehydration of erythrocytes and a resulting spiked shape. These abnormally shaped erythrocytes are preferentially trapped and destroyed by the reticuloendothelial system of the spleen. Thus, Nmnat3 deficiency in mice caused splenomegaly and hemolytic anemia (Fig. 8).

Nmnat3$^{gt/gt}$ mice manifest hemolytic anemia from a very early age, as early as four weeks. It is well known that some of metabolic enzyme deficiencies can cause congenital hemolytic

anemia in humans (49). Nmnat3$^{gt/gt}$ mice exhibit a phenotype very similar to that of pyruvate kinase (PK) -deficient mice (50,51). Among PK isoforms, liver and RBC type PK (PKLR) deficiency cause hemolytic anemia. In PK-deficient mice, a shortened lifespan of mature erythrocytes primarily contributes to hemolytic anemia pathogenesis, whereas ineffective erythropoiesis also occurs in these mice (52). Thus, it is possible that ineffective erythropoiesis may occur in Nmnat3$^{gt/gt}$ mice. To date, no *Nmnat3* gene mutation has been found in human hemolytic anemia patients. However, hemolytic anemia in Nmnat3$^{gt/gt}$ mice resembles the phenotype of PK-deficient mice. Indeed, lack of PK in mice similarly causes the glycolysis inhibition and failure of ATP production. Notably, some hemolytic anemia patients clinically showed PK-deficiency-like hemolytic anemia, but neither enzymatic deficiency nor a genetic mutation in pyruvate kinase were not found (53). Thus, it may be that an *Nmnat3* gene mutation is hidden in human patients with congenital hemolytic anemia, particularly in undiagnosed PK deficiency-like patients.

We revealed that the level of NAD of Nmnat3$^{gt/gt}$ erythrocytes was drastically decreased compared with that of WT. In addition, mild decreases of NAM and NMN were also observed in Nmnat3$^{gt/gt}$ erythrocytes. One of the explanation of these decreases is that salvage pathway in Nmnat3$^{gt/gt}$ erythrocytes is impaired. In salvage pathway, NAM is supplied from NAD by sirtuin or PARP. It is uncertain that the conversion of NAM from NAD exists in mature erythrocytes. However, an extensive proteomic analysis identified PARP10, PARP12 and ADP-ribosylhydrolase 3 (ARH3) in human erythrocyte, as well as Nmnat3 (54). This fact implied the existence of salvage pathway by PARP in mature erythrocytes, but the actual molecular identities are still unknown. Another explanation for the reduction of NAM and NMN in Nmnat3$^{gt/gt}$ erythrocytes is that the incorporation of NAM was impaired in Nmnat3$^{gt/gt}$ erythrocytes due to the deformation of plasma membrane. Indeed, PRPP, the other substrate for NMN synthesis and Nampt, a NMN synthesis enzyme, were significantly increased in Nmnat3$^{gt/gt}$ erythrocytes (Fig 6A and Fig. 5K). These results also recapture the facts that NAM and NMN were decreased in Nmnat3$^{gt/gt}$ erythrocytes. However, molecular details of NAM incorporation into mature erythrocytes are still unclear and of interest for further investigations.

In Nmnat3$^{gt/gt}$ erythrocytes, F1,6BP was markedly increased due to the reverse flow from GAP. F1,6BP is known as an allosteric activator of pyruvate kinase (55). The accumulation of F1,6BP may increase the downstream flow of glycolysis by activating PK to compensate for the reduced glycolysis in Nmnat3$^{gt/gt}$ erythrocytes. We also demonstrated that the acetylation status in Nmnat3$^{gt/gt}$ erythrocytes was increased compared with that in WT. This difference could be due to decreased NAD and increased acetyl-CoA. As it is not verified whether sirtuin is present in erythrocytes, and thus the impact of decreased NAD in the hyper acetylation of Nmnat3$^{gt/gt}$ erythrocytes is unclear. However, a recent study suggests that protein acetylation in mitochondria occurs non-enzymatically and merely increased cellular acetyl-CoA can chemically acetylate proteins (56). It was reported that cytoplasmic acetyl-CoA in erythrocytes was generated from acetate by acetyl-CoA synthetase (57). It might be possible that the blockade of glycolysis in Nmnat3$^{gt/gt}$ erythrocytes indirectly activates the acetyl CoA synthesis pathway. We measured the activity of several glycolysis and pentose phosphate pathway enzymes and found their activities to be similar or increased compared with that in WT. These results suggested that acetylation increased, or at least did not decreases, the activity of these enzymes. We can accordingly speculate that acetylation is not the cause of glycolysis inhibition in Nmnat3$^{gt/gt}$ erythrocytes but a compensatory result for decreased glycolysis. Thus, the accumulation of F1,6BP and hyper acetylation of erythrocyte proteins would be a compensatory reaction for recovering the compromised ATP production in Nmnat3$^{gt/gt}$ erythrocytes.

Although Nmnat3 is considered a mitochondrial protein, our study revealed that Nmnat3 can resides in the cytoplasm of mature erythrocytes. A previous report also indicated that Nmnat3 enzymatic activity was dominant in human

erythrocytes (35). During the final step of erythropoiesis, mitochondria are excluded from reticulocytes. However, our result showed that Nmnat3 existed in the cytoplasm even in the reticulocytes. It was reported that some mitochondrial proteins are present in mature erythrocytes (54,58). Thus, it is desirable to investigate the subcellular localization of Nmnat3 in various cell types other than erythrocytes. In addition, Nmnat3 distribution is limited to certain tissues. If Nmnat3 is responsible for mitochondrial NAD synthesis, it should be present in most cell types that possess mitochondria. Further, we found that NAD levels in liver, skeletal muscle, and heart of Nmnat3$^{gt/gt}$ mice were similar to those in WT. Nmnat3$^{gt/gt}$ mice have no other phenotypes other than hemolytic anemia at normal housed condition, pointed out an intriguing question of how the mutant mice maintain their mitochondrial NAD level at Nmnat3 absence. It is currently accepted that NAD cannot cross the inner membrane of mitochondria and may be generated in the mitochondria matrix by Nmnat3 (59,60). However, our results suggest that NAD is imported into mitochondria through an unidentified NAD transporter. Indeed, other groups have proposed such an NAD transporter (61-63). We also showed that Nmnat3$^{gt/gt}$ mice have normal hematopoiesis and erythropoiesis. In Nmnat3$^{gt/gt}$ mice, white blood cell and platelets show normal numbers and subpopulations. The Nmnat3$^{gt/gt}$ erythroblast fraction has the same amount of NAD as WT. Our results accordingly suggest that Nmnat1 and Nmnat2 can compensate for mitochondrial NAD metabolism in these cells. As told, the mechanism of mitochondrial NAD supply may be more versatile than we understood currently.

In conclusion, our study has revealed the essential role of Nmnat3 on the NAD pool maintenance in mature erythrocytes. These findings provide new tools for studying the mechanism and pathophysiology of congenital hemolytic anemia and suggest the potential of NAD metabolism as a new therapeutic target of hemolytic anemia.

ACKNOWLEDGEMENT

We are grateful to Lee DH, Shinzawa K, and Chang HC for critical reading of the manuscript and Nakagawa Lab members for discussion. We also thank to Kazuyuki Nishio and Masahiko Kawahara (Life Science Research Center, University of Toyama) for helping the scanning electron microscopy experiments and Tomomi Kubo for mice care and husbandry.

REFERENCES

1. Chiarugi, A., Dolle, C., Felici, R., and Ziegler, M. (2012) The NAD metabolome--a key determinant of cancer cell biology. *Nat Rev Cancer* **12**, 741-752
2. Houtkooper, R. H., Canto, C., Wanders, R. J., and Auwerx, J. (2010) The secret life of NAD+: an old metabolite controlling new metabolic signaling pathways. *Endocr Rev* **31**, 194-223
3. Guarente, L. (2013) Calorie restriction and sirtuins revisited. *Genes Dev* **27**, 2072-2085
4. Zhao, S., Xu, W., Jiang, W., Yu, W., Lin, Y., Zhang, T., Yao, J., Zhou, L., Zeng, Y., Li, H., Li, Y., Shi, J., An, W., Hancock, S. M., He, F., Qin, L., Chin, J., Yang, P., Chen, X., Lei, Q., Xiong, Y., and Guan, K. L. (2010) Regulation of cellular metabolism by protein lysine acetylation. *Science* **327**, 1000-1004
5. Wang, Q., Zhang, Y., Yang, C., Xiong, H., Lin, Y., Yao, J., Li, H., Xie, L., Zhao, W., Yao, Y., Ning, Z. B., Zeng, R., Xiong, Y., Guan, K. L., Zhao, S., and Zhao, G. P. (2010) Acetylation of metabolic enzymes coordinates carbon source utilization and metabolic flux. *Science* **327**, 1004-1007
6. Motta, M. C., Divecha, N., Lemieux, M., Kamel, C., Chen, D., Gu, W., Bultsma, Y., McBurney, M., and Guarente, L. (2004) Mammalian SIRT1 represses forkhead transcription factors. *Cell* **116**, 551-563

7. Purushotham, A., Schug, T. T., Xu, Q., Surapureddi, S., Guo, X., and Li, X. (2009) Hepatocyte-specific deletion of SIRT1 alters fatty acid metabolism and results in hepatic steatosis and inflammation. *Cell Metab* **9**, 327-338
8. Rodgers, J. T., Lerin, C., Haas, W., Gygi, S. P., Spiegelman, B. M., and Puigserver, P. (2005) Nutrient control of glucose homeostasis through a complex of PGC-1alpha and SIRT1. *Nature* **434**, 113-118
9. Mouchiroud, L., Houtkooper, R. H., Moullan, N., Katsyuba, E., Ryu, D., Canto, C., Mottis, A., Jo, Y. S., Viswanathan, M., Schoonjans, K., Guarente, L., and Auwerx, J. (2013) The NAD(+)/Sirtuin Pathway Modulates Longevity through Activation of Mitochondrial UPR and FOXO Signaling. *Cell* **154**, 430-441
10. Revollo, J. R., Korner, A., Mills, K. F., Satoh, A., Wang, T., Garten, A., Dasgupta, B., Sasaki, Y., Wolberger, C., Townsend, R. R., Milbrandt, J., Kiess, W., and Imai, S. (2007) Nampt/PBEF/Visfatin regulates insulin secretion in beta cells as a systemic NAD biosynthetic enzyme. *Cell Metab* **6**, 363-375
11. Yoshino, J., Mills, K. F., Yoon, M. J., and Imai, S. (2011) Nicotinamide mononucleotide, a key NAD(+) intermediate, treats the pathophysiology of diet- and age-induced diabetes in mice. *Cell Metab* **14**, 528-536
12. Lau, C., Niere, M., and Ziegler, M. (2009) The NMN/NaMN adenylyltransferase (NMNAT) protein family. *Front Biosci (Landmark Ed)* **14**, 410-431
13. Berger, F., Lau, C., Dahlmann, M., and Ziegler, M. (2005) Subcellular compartmentation and differential catalytic properties of the three human nicotinamide mononucleotide adenylyltransferase isoforms. *J Biol Chem* **280**, 36334-36341
14. Di Stefano, M., and Conforti, L. (2013) Diversification of NAD biological role: the importance of location. *FEBS J* **280**, 4711-4728
15. Chiang, P. W., Wang, J., Chen, Y., Fu, Q., Zhong, J., Chen, Y., Yi, X., Wu, R., Gan, H., Shi, Y., Chen, Y., Barnett, C., Wheaton, D., Day, M., Sutherland, J., Heon, E., Weleber, R. G., Gabriel, L. A., Cong, P., Chuang, K., Ye, S., Sallum, J. M., and Qi, M. (2012) Exome sequencing identifies NMNAT1 mutations as a cause of Leber congenital amaurosis. *Nat Genet* **44**, 972-974
16. Koenekoop, R. K., Wang, H., Majewski, J., Wang, X., Lopez, I., Ren, H., Chen, Y., Li, Y., Fishman, G. A., Genead, M., Schwartzentruber, J., Solanki, N., Traboulsi, E. I., Cheng, J., Logan, C. V., McKibbin, M., Hayward, B. E., Parry, D. A., Johnson, C. A., Nageeb, M., Finding of Rare Disease Genes Canada, C., Poulter, J. A., Mohamed, M. D., Jafri, H., Rashid, Y., Taylor, G. R., Keser, V., Mardon, G., Xu, H., Inglehearn, C. F., Fu, Q., Toomes, C., and Chen, R. (2012) Mutations in NMNAT1 cause Leber congenital amaurosis and identify a new disease pathway for retinal degeneration. *Nat Genet* **44**, 1035-1039
17. Perrault, I., Hanein, S., Zanlonghi, X., Serre, V., Nicouleau, M., Defoort-Delhemmes, S., Delphin, N., Fares-Taie, L., Gerber, S., Xerri, O., Edelson, C., Goldenberg, A., Duncombe, A., Le Meur, G., Hamel, C., Silva, E., Nitschke, P., Calvas, P., Munnich, A., Roche, O., Dollfus, H., Kaplan, J., and Rozet, J. M. (2012) Mutations in NMNAT1 cause Leber congenital amaurosis with early-onset severe macular and optic atrophy. *Nat Genet* **44**, 975-977
18. Falk, M. J., Zhang, Q., Nakamaru-Ogiso, E., Kannabiran, C., Fonseca-Kelly, Z., Chakarova, C., Audo, I., Mackay, D. S., Zeitz, C., Borman, A. D., Staniszewska, M., Shukla, R., Palavalli, L., Mohand-Said, S., Waseem, N. H., Jalali, S., Perin, J. C., Place, E., Ostrovsky, J., Xiao, R., Bhattacharya, S. S., Consugar, M., Webster, A. R., Sahel, J. A., Moore, A. T., Berson, E. L., Liu, Q., Gai, X., and Pierce, E. A. (2012) NMNAT1 mutations cause Leber congenital amaurosis. *Nat Genet* **44**, 1040-1045
19. Mack, T. G., Reiner, M., Beirowski, B., Mi, W., Emanuelli, M., Wagner, D., Thomson, D., Gillingwater, T., Court, F., Conforti, L., Fernando, F. S., Tarlton, A., Andressen, C., Addicks, K., Magni, G., Ribchester, R. R., Perry, V. H., and Coleman, M. P. (2001) Wallerian

degeneration of injured axons and synapses is delayed by a Ube4b/Nmnat chimeric gene. *Nat Neurosci* **4**, 1199-1206

20. Sasaki, Y., Vohra, B. P., Baloh, R. H., and Milbrandt, J. (2009) Transgenic mice expressing the Nmnat1 protein manifest robust delay in axonal degeneration in vivo. *J Neurosci* **29**, 6526-6534
21. Conforti, L., Janeckova, L., Wagner, D., Mazzola, F., Cialabrini, L., Di Stefano, M., Orsomando, G., Magni, G., Bendotti, C., Smyth, N., and Coleman, M. (2011) Reducing expression of NAD+ synthesizing enzyme NMNAT1 does not affect the rate of Wallerian degeneration. *FEBS J* **278**, 2666-2679
22. Gilley, J., and Coleman, M. P. (2010) Endogenous Nmnat2 is an essential survival factor for maintenance of healthy axons. *PLoS Biol* **8**, e1000300
23. Yan, T., Feng, Y., Zheng, J., Ge, X., Zhang, Y., Wu, D., Zhao, J., and Zhai, Q. (2010) Nmnat2 delays axon degeneration in superior cervical ganglia dependent on its NAD synthesis activity. *Neurochem Int* **56**, 101-106
24. Hicks, A. N., Lorenzetti, D., Gilley, J., Lu, B., Andersson, K. E., Miligan, C., Overbeek, P. A., Oppenheim, R., and Bishop, C. E. (2012) Nicotinamide mononucleotide adenylyltransferase 2 (Nmnat2) regulates axon integrity in the mouse embryo. *PLoS One* **7**, e47869
25. Gilley, J., Adalbert, R., Yu, G., and Coleman, M. P. (2013) Rescue of peripheral and CNS axon defects in mice lacking NMNAT2. *J Neurosci* **33**, 13410-13424
26. Nikiforov, A., Dolle, C., Niere, M., and Ziegler, M. (2011) Pathways and subcellular compartmentation of NAD biosynthesis in human cells: from entry of extracellular precursors to mitochondrial NAD generation. *J Biol Chem* **286**, 21767-21778
27. Sasaki, Y., Araki, T., and Milbrandt, J. (2006) Stimulation of nicotinamide adenine dinucleotide biosynthetic pathways delays axonal degeneration after axotomy. *J Neurosci* **26**, 8484-8491
28. Yahata, N., Yuasa, S., and Araki, T. (2009) Nicotinamide mononucleotide adenylyltransferase expression in mitochondrial matrix delays Wallerian degeneration. *J Neurosci* **29**, 6276-6284
29. Preiss, J., and Handler, P. (1957) Enzymatic synthesis of nicotinamide mononucleotide. *J Biol Chem* **225**, 759-770
30. Micheli, V., and Sestini, S. (1997) Determining NAD synthesis in erythrocytes. *Methods Enzymol* **280**, 211-221
31. Micheli, V., Simmonds, H. A., Sestini, S., and Ricci, C. (1990) Importance of nicotinamide as an NAD precursor in the human erythrocyte. *Arch Biochem Biophys* **283**, 40-45
32. Micheli, V., Sestini, S., Rocchigiani, M., Pescaglini, M., and Ricci, C. (1991) Significance and relevance of NAD synthesis in human erythrocyte life span. *Adv Exp Med Biol* **307**, 139-146
33. Sestini, S., Ricci, C., Micheli, V., and Pompucci, G. (1993) Nicotinamide mononucleotide adenylyltransferase activity in human erythrocytes. *Arch Biochem Biophys* **302**, 206-211
34. Liu, R., and Orgel, L. E. (1995) Enzymatic synthesis of polymers containing nicotinamide mononucleotide. *Nucleic Acids Res* **23**, 3742-3749
35. Di Stefano, M., Galassi, L., and Magni, G. (2010) Unique expression pattern of human nicotinamide mononucleotide adenylyltransferase isozymes in red blood cells. *Blood Cells Mol Dis* **45**, 33-39
36. Noble, N. A., Xu, Q. P., and Ward, J. H. (1989) Reticulocytes. I. Isolation and in vitro maturation of synchronized populations. *Blood* **74**, 475-481
37. Manodori, A. B., and Kuypers, F. A. (2002) Altered red cell turnover in diabetic mice. *J Lab Clin Med* **140**, 161-165
38. Orsomando, G., Cialabrini, L., Amici, A., Mazzola, F., Ruggieri, S., Conforti, L., Janeckova, L., Coleman, M. P., and Magni, G. (2012) Simultaneous single-sample determination of

NMNAT isozyme activities in mouse tissues. *PLoS One* **7**, e53271

39. Beutler, E., Blume, K. G., Kaplan, J. C., Lohr, G. W., Ramot, B., and Valentine, W. N. (1977) International Committee for Standardization in Haematology: recommended methods for red-cell enzyme analysis. *Br J Haematol* **35**, 331-340
40. Yamada, K., Hara, N., Shibata, T., Osago, H., and Tsuchiya, M. (2006) The simultaneous measurement of nicotinamide adenine dinucleotide and related compounds by liquid chromatography/electrospray ionization tandem mass spectrometry. *Anal Biochem* **352**, 282-285
41. Darghouth, D., Koehl, B., Madalinski, G., Heilier, J. F., Bovee, P., Xu, Y., Olivier, M. F., Bartolucci, P., Benkerrou, M., Pissard, S., Colin, Y., Galacteros, F., Bosman, G., Junot, C., and Romeo, P. H. (2011) Pathophysiology of sickle cell disease is mirrored by the red blood cell metabolome. *Blood* **117**, e57-66
42. Sporty, J. L., Kabir, M. M., Turteltaub, K. W., Ognibene, T., Lin, S. J., and Bench, G. (2008) Single sample extraction protocol for the quantification of NAD and NADH redox states in Saccharomyces cerevisiae. *J Sep Sci* **31**, 3202-3211
43. Yuan, M., Breitkopf, S. B., Yang, X., and Asara, J. M. (2012) A positive/negative ion-switching, targeted mass spectrometry-based metabolomics platform for bodily fluids, cells, and fresh and fixed tissue. *Nat Protoc* **7**, 872-881
44. Felici, R., Lapucci, A., Ramazzotti, M., and Chiarugi, A. (2013) Insight into Molecular and Functional Properties of NMNAT3 Reveals New Hints of NAD Homeostasis within Human Mitochondria. *PLoS One* **8**, e76938
45. van den Bos, C., Kieboom, D., Visser, T. P., and Wagemaker, G. (1993) Compensatory splenic hemopoiesis in beta-thalassemic mice. *Exp Hematol* **21**, 350-353
46. Loken, M. R., Shah, V. O., Dattilio, K. L., and Civin, C. I. (1987) Flow cytometric analysis of human bone marrow: I. Normal erythroid development. *Blood* **69**, 255-263
47. Stanton, R. C. (2012) Glucose-6-phosphate dehydrogenase, NADPH, and cell survival. *IUBMB Life* **64**, 362-369
48. Liu, J., Mohandas, N., and An, X. (2011) Membrane assembly during erythropoiesis. *Curr Opin Hematol* **18**, 133-138
49. Climent, F., Roset, F., Repiso, A., and Perez de la Ossa, P. (2009) Red cell glycolytic enzyme disorders caused by mutations: an update. *Cardiovasc Hematol Disord Drug Targets* **9**, 95-106
50. Kanno, H., Morimoto, M., Fujii, H., Tsujimura, T., Asai, H., Noguchi, T., Kitamura, Y., and Miwa, S. (1995) Primary structure of murine red blood cell-type pyruvate kinase (PK) and molecular characterization of PK deficiency identified in the CBA strain. *Blood* **86**, 3205-3210
51. Morimoto, M., Kanno, H., Asai, H., Tsujimura, T., Fujii, H., Moriyama, Y., Kasugai, T., Hirono, A., Ohba, Y., Miwa, S., and Kitamura, Y. (1995) Pyruvate kinase deficiency of mice associated with nonspherocytic hemolytic anemia and cure of the anemia by marrow transplantation without host irradiation. *Blood* **86**, 4323-4330
52. Aizawa, S., Harada, T., Kanbe, E., Tsuboi, I., Aisaki, K., Fujii, H., and Kanno, H. (2005) Ineffective erythropoiesis in mutant mice with deficient pyruvate kinase activity. *Exp Hematol* **33**, 1292-1298
53. Miwa, S., Kanno, H., and Fujii, H. (1993) Concise review: pyruvate kinase deficiency: historical perspective and recent progress of molecular genetics. *Am J Hematol* **42**, 31-35
54. Roux-Dalvai, F., Gonzalez de Peredo, A., Simo, C., Guerrier, L., Bouyssie, D., Zanella, A., Citterio, A., Burlet-Schiltz, O., Boschetti, E., Righetti, P. G., and Monsarrat, B. (2008) Extensive analysis of the cytoplasmic proteome of human erythrocytes using the peptide ligand library technology and advanced mass spectrometry. *Mol Cell Proteomics* **7**, 2254-2269

55. Kirtley, M. E., and McKay, M. (1977) Fructose-1,6-bisphosphate, a regulator of metabolism. *Mol Cell Biochem* **18**, 141-149
56. Wagner, G. R., and Payne, R. M. (2013) Widespread and enzyme-independent Nepsilon-acetylation and Nepsilon-succinylation of proteins in the chemical conditions of the mitochondrial matrix. *J Biol Chem* **288**, 29036-29045
57. Pittman, J. G., and Martin, D. B. (1966) Fatty acid biosynthesis in human erythrocytes: evidence in mature erythrocytes for an incomplete long chain fatty acid synthesizing system. *J Clin Invest* **45**, 165-172
58. Tyan, Y. C., Jong, S. B., Liao, J. D., Liao, P. C., Yang, M. H., Liu, C. Y., Klauser, R., Himmelhaus, M., and Grunze, M. (2005) Proteomic profiling of erythrocyte proteins by proteolytic digestion chip and identification using two-dimensional electrospray ionization tandem mass spectrometry. *J Proteome Res* **4**, 748-757
59. Stein, L. R., and Imai, S. (2012) The dynamic regulation of NAD metabolism in mitochondria. *Trends Endocrinol Metab* **23**, 420-428
60. Dolle, C., Rack, J. G., and Ziegler, M. (2013) NAD and ADP-ribose metabolism in mitochondria. *FEBS J* **280**, 3530-3541
61. Haferkamp, I., Schmitz-Esser, S., Linka, N., Urbany, C., Collingro, A., Wagner, M., Horn, M., and Neuhaus, H. E. (2004) A candidate NAD+ transporter in an intracellular bacterial symbiont related to Chlamydiae. *Nature* **432**, 622-625
62. Palmieri, F., Rieder, B., Ventrella, A., Blanco, E., Do, P. T., Nunes-Nesi, A., Trauth, A. U., Fiermonte, G., Tjaden, J., Agrimi, G., Kirchberger, S., Paradies, E., Fernie, A. R., and Neuhaus, H. E. (2009) Molecular identification and functional characterization of Arabidopsis thaliana mitochondrial and chloroplastic NAD+ carrier proteins. *J Biol Chem* **284**, 31249-31259
63. Song, E. K., Rah, S. Y., Lee, Y. R., Yoo, C. H., Kim, Y. R., Yeom, J. H., Park, K. H., Kim, J. S., Kim, U. H., and Han, M. K. (2011) Connexin-43 hemichannels mediate cyclic ADP-ribose generation and its Ca2+-mobilizing activity by NAD+/cyclic ADP-ribose transport. *J Biol Chem* **286**, 44480-44490

FOOTNOTES

This work is supported by a Grant-in-Aid for Young Scientists (A) (24609019) and a Grant-in-Aid for Scientific Research on Innovative Areas (24116511) to T.N. This work is also supported by a grant from The Sumitomo Foundation, a grant from Kanae Foundation for the Promotion of Medical Science, a grant from Astellas Foundation for Research on Metabolic Disorders, and a grant from Takeda Science Foundation to T.N. The authors declare no competing financial interests.

FIGURE LEGENDS

Table 1. Primers for Nmnat3$^{gt/gt}$ mice genotyping and mouse Nmnat3 qPCR. Locations of the primers used in geneotyping for Nmnat3$^{gt/gt}$ mice are indicated in Figure 2A. Locations of the primers used for qPCR of Nmnat3 mRNA are indicated in Figure 2B.

Table 2. Hematological examination reveals Nmnat3$^{gt/gt}$ mice are anemic, but not pancytopenia. Peripheral blood cell numbers and various hematological parameters were counted in 12 weeks old WT and Nmnat3$^{gt/gt}$ mice (n = 4 for each group). All data are expressed as mean ± SD. The abbreviations used are as follows: RBC, red blood cell; Hb, hemoglobin; HCT, hematocrit; MCV, mean corpuscle volume; MCH, mean corpuscle hemoglobin; MCHC, mean corpuscle hemoglobin concentration; WBC, white blood cell; Neu, neutrophil; Lym, lymphocyte; Ba, basophil; Eo, eosinophil; Mo, monocyte; PLT, platelet.

Figure 1. Nmnat3 exists in cytoplasmic fraction of mature erythrocytes. (A) Immunoblot analysis of Nmnat3 expression in indicated tissues from wild-type (WT) mouse. β-Actin, β-Tubulin and GAPDH were used as loading controls. (B) Immunofluorescent images of human NMNAT3-Flag over-expressed Hela cells (Right panel). DsRed2-Mito was co-transfected and used as mitochondrial marker (red). NMNAT3-Flag (green) was visualized by anti-Flag M2 antibody. NMNAT3-Flag expression was also confirmed by Western blotting with anti-Flag M2 antibody (Left panel). (C) Fractionation experiment of mature erythrocyte using WT mouse. GAPDH was used as a cytoplasm fraction marker. Ter119 and β-Actin were used as membrane fraction markers. Nmnat3 was detected in the cytoplasm fraction. (D) Fractionation experiment of reticulocyte using WT mouse. GAPDH was used as a cytoplasm fraction marker. Tom20 was used as mitochondrial fraction markers. Nmnat3 was detected in the cytoplasm fraction.

Figure 2. Nmnat3$^{gt/gt}$ mice exhibit splenomegaly and hemolytic anemia. (A) Map of Nmnat3 gene-trapped allele. The gene-trap cassette was inserted into the indicated point between *Nmnat3* gene exon 1 and exon 2. (B) Structure of Nmnat3 mRNA generated from WT and Nmnat3 gene-trapped allele. The abbreviations used are as follows: SA, splicing acceptor; β-geo, β-galactosidase and neomycin resistance cassette fusion gene; pA, poly-A. (C) Genotyping PCR of Nmnat3 gene-trap homozygous mice (Nmnat3$^{gt/gt}$ mice). Primer sets are shown as green arrow in (A). These primer sets successfully amplified 340 bp, 675 bp and 184 bp PCR products for wild type allele, 5' end and 3' end of gene-targeted allele, respectively. (D-F) Real-time quantitative PCR analysis of Nmnat3 mRNA using primer sets to detect exon1, exon2-3 junction, or exon5. Total RNA was prepared from skeletal muscle (D), heart (E) and liver (F). Data are presented as mean ± SD (n = 4 for each group). (G and H) Immunoblot analysis of Nmnat3 in RBC (G) and skeletal muscle (H) prepared from WT and Nmnat3$^{gt/gt}$ mice. β-Actin or β-Tubulin was used as a loading control. Arrowhead indicates the Nmnat3 band (~30 kDa). (I) Representative picture of spleens from 8-week-old WT and Nmnat3$^{gt/gt}$ mice. (J) Ratio of spleen and body weight was calculated using WT and Nmnat3$^{gt/gt}$ mice (n = 4 for each group). (K) Hematoxylin-Eosin (HE) staining of spleen section prepared from WT and Nmnat3$^{gt/gt}$ mice. Hemosiderin deposit was seen in the enlarged lower left corner. Scale bar represents 50 μm. (L) May-Giemsa and New Methylene Blue staining of peripheral blood collected from WT and Nmnat3$^{gt/gt}$ mice. Scale bar represents 20 μm. (M) Representative scanning electron microscope image of erythrocytes prepared from WT and Nmnat3$^{gt/gt}$ mice. Experiments were independently repeated three times. (N) RBCs of 12-week old mice (n = 3 for each group) were biotinylated by tail vein injection of EZ-Link Sulfo-NHS-biotin and blood was drawn at indicated time. RBC was labeled with phycoerythrin (PE)-conjugated streptavidin and quantified by flow cytometry. Data are presented as mean ± SD. (n = 3 for each group)

Figure 3. Erythropoiesis is compensatory up regulated, but normal in Nmnat3$^{gt/gt}$ mice. (A-C) Flow cytometer analysis for erythroid differentiation stage. Splenocytes (A), bone marrow cells (B), and peripheral blood (C) prepared from 8-week-old WT and Nmnat3$^{gt/gt}$ mice were analyzed by the expression of erythroid cell surface marker Ter119 and CD71 with flow cytometer. The representative data are shown in left panel for each cell types. P4 (Ter119^{high}/ CD71^{high}), P5 (Ter119^{high}/ CD71^{middle}), and P6 (Ter119^{high}/ CD71^{low}) populations were calculated as percent of total (right graph). Data are presented as mean ± SD. (n = 4 for each group) (D) Whole blood cells were stained with Hoechst 33342 and MitoTracker Orange for nucleus and mitochondria, respectively. Cells stained with Hoechst 33342 are indicated by arrow. Phase contrast image (DIC) was shown in left panel.

Figure 4. Nmnat3 is a dominant Nmnat isozyme in mature erythrocytes. (A) Nmnat3-specific activity and total Nmnat activity of mature erythrocytes were determined by discrimination assay with $CoCl_2$ and $MgCl_2$, respectively. For this assay, mature erythrocytes lysates were prepared from WT and Nmnat3$^{gt/gt}$ mice. Samples were dialyzed to remove endogenous metal ion and metabolites. Data are presented as mean ± SD (n = 3 for each group). (B) Immunoblot analysis of endogenous Nmnat1 and Nmnat2 protein in mature erythrocyte with Nmnat1 and Nmnat2 specific antibody. Total cell lysates from mouse Nmnat1 or Nmnat2 over-expressed NIH3T3 cells were used as positive control.

Figure 5. NAD pool in mature erythrocytes is drastically reduced in Nmnat3$^{gt/gt}$ mice. (A) Representative chromatograms of NAD in RBC samples prepared from WT and Nmnat3$^{gt/gt}$ mice. (B and C) Absolute quantification of NAD (B) and NADH (C) level in RBC prepared from 8-week-old WT and Nmnat3$^{gt/gt}$ mice. The concentration was calculated from peak area using standard curve and expressed as defined unit. Data are presented as mean ± SD (n = 4 for each group). (D) Absolute quantification of NAD level in whole blood prepared from 8-week-old WT and Nmnat3$^{gt/gt}$ mice. The concentration was calculated from peak area using standard curve and expressed as defined unit. Data are presented as mean ± SD (n = 4 for each group). (E and F) Semi-quantification of NAD related metabolites in RBC (E) or whole blood (F). NAM (Nicotinamide), NMN (Nicotinamide mononucleotide), NAD (Nicotinamide adenine dinucleotide), NA (Nicotinic acid), NAMN (Nicotinic acid mononucleotide), NAAD (Nicotinic acid adenine dinucleotide), and NR (Nicotinamide riboside) were measured by LC-MS/MS. Data are presented as mean ± SD (n = 4 for each group). N.D. means not detected. (G) NAD amount was measured in heart, liver and skeletal muscle. NAD amount was normalized by wet tissue weight. Data are presented as mean ± SD (n = 4 for each group). (H) Representative result of FACS sorting. Splenocytes from WT and Nmnat3$^{gt/gt}$ mice were stained with anti-CD71-FITC and anti-Ter119-PE, and were sorted by FACS Aria with defined gates. (I) P4 (Ter119^{high}/ CD71^{high}), P5 (Ter119^{high}/ CD71^{middle}), and P6 (Ter119^{high}/ CD71^{low}) sub-populations of splenocytes were sorted, and NAD level in these samples were measured by LC-MS/MS. Data are presented as mean ± SD (n = 4 for each group). (J) Absolute quantification of NADP in RBC. NADP was measured by LC-MS/MS. The concentration was calculated from peak area using standard curve and expressed as defined unit. Data are presented as mean ± SD (n = 4 for each group). (K) Immunoblot analysis of NADK and Nampt in mature erythrocytes from WT and Nmnat3$^{gt/gt}$ mice. β-Actin was used as a loading control. Arrowhead indicates the NADK band (~50 kDa). Proteins were extracted from three mice for each groups. (L) GSH (reduced glutathione) and GSSG (oxidized glutathione) in RBC were measured by LC-MS/MS. Data are presented as mean ± SD (n = 4 for each group).

Figure 6. Glycolysis pathway is blocked in Nmnat3$^{gt/gt}$ erythrocytes. (A) Metabolites in glycolysis pathway and pentose phosphate pathway were measured using RBC samples obtained from 8-week-old WT and Nmnat3$^{gt/gt}$ mice (n = 4 for each group). G6P/F6P (Glucose 6-phospate / Fructose 6-phospate), F1,6BP (Fructose 1,6-bisphosphate), DHAP (Dihydroxyacetone phosphate), GAP (Glyceraldehyde 3-phosphate), 2,3-BPG (2,3-bisphospho glycerate), 3PG (3-phosphoglycerate), PEP